1. Research on improvement of GaN-based light emitting devices grown on silicon (111) substrate
(シリコン(111)基板上窒化ガリウム系発光デバイスの特性改善に関する研究)

1. Introduction

1.1 Introduction

In the end of 20th century, progress in silicon fabrication technology has created information society through rapid progress in information technology (IT) industry. Progress in IT industry further demanded for immediate and low-latency access for large volume of data which then merged into information and communication technology (ICT). Worldwide spreading of internet is the core factor which pushed rapid development in the industry. Since the early 21st century, a new ubiquitous society has started to be born through the advancement in ICT industry. In ubiquitous society, access to information is "anytime, anywhere, with anyone and with anything".

As a result for information accessibility by the society, copper-based cable communication can no longer serve the large volume of information at low-latency, which then pushes for optical-based communication like fiber-optics. Cell phone previously a medium for voice communication has emerged into smart phone which carries voice, video and data communications, demanding for more base stations with more efficient use of wavelength to serve the growing volume of data transmission. Radio and video broadcast through analog wave signal need to be converted into digital signal to significantly improve radio wave utilization, while at the same time broadcasting more information with better quality to the audiences. Vehicles previously a solely mechanical products with combustion engine, have emerged into smart vehicles with mechanical-electrical hybrid engine, supported by intelligent transportation system (ITS) for improved safety, security and efficiency in surface transportation system.

Ubiquitous society has demanded for enormous utilization of resources and electricity. The vast amounts of data also need to be efficiently stored and archived, which demanded for higher density data storage.

Optoelectronic devices such as light emitting diode (LED) and laser diode (LD) play a very important role in telecommunication, data storage, printing, display, etc. GaAs and InP-based materials have long been used for LED and LD applications in red, near infra-red (NIR) and infra-red (IR) light region. LD with 1.3-1.5 μm wavelength band is being used in optical communications, while LD with 650 nm wavelength is being used in data storage such as digital versatile disc (DVD).

Research breakthroughs by H. P. Maruska, I. Akasaki, and S. Nakamura groups in 1970s until 1990s have led to successful material growth and device fabrication for gallium nitride (GaN)-based III-nitride electronics and optoelectronic devices. GaN-based semiconductor is highly anticipated as one of the most important materials to solve many problems related to demands in recent ubiquitous society.

III-nitride-based materials can be applied in wide area of optoelectronics and electronics products. As shown in Fig. 1.1, the wide band-gap energy of III-nitride alloys from 0.7 eV for InN to 6.2 eV for AlN can cover the whole light spectrum from deep ultra-violet (DUV) until IR region, therefore giving high expectations for applications in light emission devices such as LED and LD. InGaN-based active layer has been used for fabrication of high-brightness blue and green LED [1-2]. AlInGaN-based quaternary active layer is used in fabrication of UV-LED shorter than 365 nm wavelength [3-4]. InGaN-based active layer with emission wavelength at 400 nm has also been applied in LD for high-density Blu-ray DVD (BD) standard [5-6].

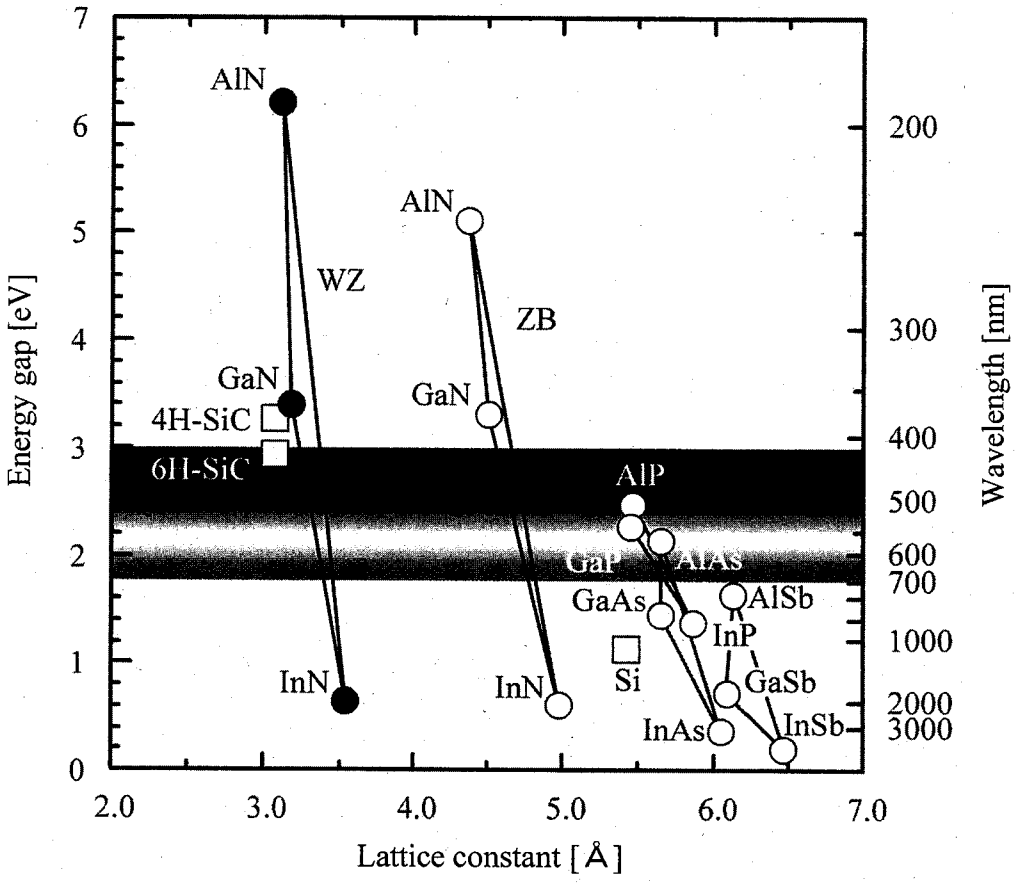

Fig. 1.1. Band-gap energy as a function of lattice constant for common semiconductor materials.

1.2 Progress of III-Nitride Research

Growth of GaN on sapphire substrate was first reported by H. P. Maruska *et al.* from Radio Corporation of America (RCA) Laboratories in 1969 [7]. HCl and Ga as the source for group-III material were flowed together in carrier gas, forming GaCl and $GaCl_3$ group-III halide by using halide vapor phase epitaxy growth method. The growth method is also known as hydride vapor phase epitaxy (HVPE) because hydride-based ammonia (NH_3) is used as source material for group-V. It has been determined that GaN has a direct energy band-gap of 3.39 eV and the GaN film was n-type with electron concentration typically above 10^{19} cm^{-3} without intentional doping. A great interest for application in blue-violet light emitting devices was born from this discovery. J. I. Pankove *et al.* reported first blue-LED with n-type single-crystal GaN using metal-insulator-semiconductor (MIS) structure [8]. However, the operation voltage was very high and external quantum efficiency (η_{eqe}) at 430-490 nm emission wavelength was just around 0.02 – 0.12% [9-10], which is very low compared to LED emitting at other wavelength regions. GaN film grown at that time has (1) poor surface flatness and many cracks, (2) relatively high deep-level emission resulted from crystal defects compared to band-edge emission, and (3) high residual donor impurities creating strong unintentional n-type film even without any doping, thus realizing p-type GaN film for p-n junction was difficult.

In 1983, Yoshida *et al.* were able to obtain a strong band-edge emission by coating single-crystal AlN on sapphire substrate prior to GaN growth, using gas-source molecular beam epitaxy (MBE) [11]. However, residual electron concentration was still high at 10^{19} cm^{-3} with low electron mobility of 35 $cm^2V^{-1}s^{-1}$. High quality GaN film

was only possible in 1986 by Amano *et al.* using low-temperature AlN buffer layer using metal organic chemical vapor deposition (MOCVD) growth [12]. Using this method, a crack-free flat surface crystal growth for GaN was made possible. Furthermore, the sample also showed a weaker deep-level emission caused by crystal defects, and a lower residual electron concentration, which made control of electronic conductivity in GaN to be nearly possible. Low-temperature AlN buffer layer has solved problem (1) to (3) stated earlier, and rapidly improves electrical and optical characteristics in GaN-based materials which acts as foundation for further growth of GaN research [13].

In 1988, Amano *et al.* reported that a remarkable change in emission characteristics was observed when a MOCVD grown Zn-doped GaN (GaN:Zn) was treated by low-energy electron beam irradiation (LEEBI) [14]. In the following year, Amano *et al.* reported that the LEEBI treatment not only improved emission characteristics, but also drastically improved electrical characteristics in Mg-doped GaN (GaN:Mg) [15]. From this invention, p-type GaN was realized, and GaN-based p-n junction LED was reported for the first time which shows a great improvement in operating voltage compared to MIS-type LED reported previously [15].

Afterwards, Nakamura reported high-quality GaN film using low-temperature GaN buffer layer, which shows electron density of 4×10^{16} cm^{-3} and electron mobility of 600 $cm^2V^{-1}s^{-1}$ at room-temperature (RT), and electron density of 8×10^{15} cm^{-3} and electron mobility of 1500 $cm^2V^{-1}s^{-1}$ at 77 K [16]. Furthermore, Nakamura *et al.* discovered that Mg-doped GaN can be activated by heat-treatment in nitrogen-gas ambient to form a p-type GaN [17]. This method gives big impact on improving efficiency in mass-production environment.

InGaN which has a smaller band-gap than GaN is important for light-emitters in visible light region. InGaN film was previously grown at low temperature lower than 650 °C, which shows poor crystal quality and no report on light emission characteristics [18]. In 1991, Yoshimoto *et al.* reported growth of InGaN at higher temperature of 800 °C, and successfully obtained a good quality InGaN film with low-pressure growth at 76 Torr, with NH_3 flow of 20 l/min and V/III ratio of 20000 [19]. On the other hand, Nakamura *et al.* reported better material properties of InGaN with growth temperature between 780 to 830 °C [20]. A sharp band-edge emission with full-width at half-maximum in the range of 70-110 meV in 400-450 nm wavelength region was observed, with smaller deep-level emission reported by Yoshimoto *et al.*, which confirm a high-quality InGaN film [20]. It is then reported that a high V/III ratio and high N_2 pressure is necessary for InGaN growth [21,22]. Investigation on application of InGaN as active region in LED proceeded [23,24], and in 1994, Nakamura *et al.* reported 1 cd class high-brightness LED using p-n junction made of InGaN/AlGaN hetero-structure in the active region [25]. The emission wavelength was 450 nm with η_{eqe} of 2.7% at 20 mA operating current. Development of blue LED emission at 450 nm [26], green LED at 525 nm [27], and with the successful realization of quantum well (QW) structure, high brightness LED was realized, such as 12 cd InGaN-based green LED which was 100 times brighter than 0.1 cd GaP-based LED [28]. Mass-production of these LEDs was started in April 1994, which then allows realization of high-brightness outdoor full-color display. In 1996, Nakamura *et al.* reported first RT pulse-oscillation GaN-based laser diode (LD) using InGaN-based multi quantum well (MQW) structure [5]. Shortly in the same year, RT CW-oscillation GaN-based LD was reported by the same group [29]. Improvement in lifetime of GaN-based LD was achieved by using

epitaxial lateral overgrowth (ELO) method allowing the LD lifetime to exceed 10,000 hours [30].

1.3 Research Objective and Organization of Dissertation

This research concentrates on improving the characteristics of GaN-based light emitting devices grown on Si(111) substrate, by insertion of $Al_{0.06}Ga_{0.94}N$/GaN strained-layer superlattices (SLS) cladding underlayer prior to the growth of InGaN-based MQW active layer. The work results a significant improvement in controlling threading dislocations (TDs), internal quantum efficiency (η_{iqe}), light emission characteristics and electrical characteristics.

The dissertation composed of six chapters and each of them is summarized as follows.

Chapter 1 gives brief introduction about the technological progress which demands for a more cost efficient electronic and optoelectronic devices, such as in high-density storage, general lighting, illumination, etc. A brief explanation on progress of GaN research is also described.

In chapter 2, a few established growth techniques are described for GaN-based epitaxy on major substrates such as sapphire, Si, SiC and GaN free-standing substrate. Further detailed growth mechanism for GaN hetero-epitaxy on Si substrate is also explained, which is the fundamental subject for this research. Demand for GaN-based electronic and optoelectronic devices grown on low-cost Si substrate is emphasized to meet the challenging progress of the industry.

Chapter 3 describes major characterization method essential for GaN-based

thin-film epitaxy and devices, such as, X-ray diffraction (XRD), photoluminescence (PL), transmission electron microscopy (TEM) and device characterization method. Emphasize is made for conventional characteristics that should be expected from GaN thin-film grown by MOCVD method.

Major investigation for the effect of $Al_{0.06}Ga_{0.94}N$/GaN SLS underlayer prior to InGaN-based MQW growth is described in chapter 4. The first section of the chapter characterizes $Al_{0.06}Ga_{0.94}N$/GaN SLS underlayer relative to normal $Al_{0.03}Ga_{0.97}N$ cladding underlayer. The second section in the chapter analyzes $Al_{0.06}Ga_{0.94}N$/GaN SLS underlayer relative to conventional GaN layer, which is normally used in LED fabrication. The study also suggests mechanism for improvement in MQW light emission by the insertion of the $Al_{0.06}Ga_{0.94}N$/GaN SLS underlayer. The third section analyzes LD structure grown on Si(111) substrate with AlGaN bulk cladding layer and AlGaN/GaN SLS cladding layer. A standard LD structure grown on GaN(0001) free-standing substrate is also shown for comparison.

In chapter 5, fabrication and device evaluation of blue LED grown on Si(111) substrate is performed, with insertion of $Al_{0.06}Ga_{0.94}N$/GaN SLS underlayer, relative to conventional structure without the underlayer.

Achievements from the work in this research are summarized in chapter 6. Furthermore, suggestions for further improvements in epitaxial quality and device performance are also included in the chapter.

References

[1] S. Nakamura, T. Mukai, and M. Senoh, Appl. Phys. Lett. **64**, 1687 (1994).

[2] S. Nakamura, M. Senoh, N. Iwasa, S. Nagahama, T. Yamada, and T. Mukai, Jpn. J. Appl. Phys. **34**, L1332 (1995).

[3] M. A. Khan, V. Adivaharan, J. P. Zhang, C. Chen, E. Kuokstis, A. Chitnis, M. Shatalov, J. W. Yang, and G. Simin, Jpn. J. Appl. Phys. **40**, L1308 (2001).

[4] H. Hirayama, J. Appl. Phys. **97**, 091101 (2005).

[5] S. Nakamura, M. Senoh, S. Nagahama, N. Iwasa, T. Yamada, T. Matsushita, H. Kiyoku, and Y. Sugimoto, Jpn. J. Appl. Phys. **35**, L74 (1996).

[6] S. Nakamura, M. Senoh, S. Nagahama, N. Iwasa, T. Yamada, T. Matsushita, H. Kiyoku, Y. Sugimoto, T. Kozaki, H. Umemoto, M. Sano, and K. Chocho, Appl. Phys. Lett. **72**, 2014 (1998).

[7] H. P. Maruska, and J. J. Tietjen, Appl. Phys. Lett. **15**, 327 (1969).

[8] J. I. Pankove, E. A. Miller, D. Richman, and J. E. Berkeyheiser, J. Lumin. **4**, 63 (1971).

[9] H. P. Maruska, W. C. Rhines, and D. A. Stevenson, Mater. Res. Bull. **7**, 777 (1972).

[10] Y. Ohki, Y. Toyoda, H. Kobayashi, and I. Akasaki, Inst. Phys. Conf. Ser. **63**, 479 (1981).

[11] S. Yoshida, S. Misawa, and S. Gonda, Appl. Phys. Lett. **42**, 427 (1983).

[12] H. Amano, N. Sawaki, I. Akasaki, and Y. Toyoda, Appl. Phys. Lett. **48**, 353 (1986).

[13] I. Akasaki, H. Amano, Y. Koide, K. Hiramatsu, and N. Sawaki, J. Cryst. Growth **98**, 209 (1989).

[14] H. Amano, I. Akasaki, T. Kozawa, K. Hiramatsu, N. Sawaki, K. Ikeda, and Y. Ishii,

J. Lumin. **40 & 41**, 121 (1988).

[15] H. Amano, M. Kito, K. Hiramatsu, and I. Akasaki, Jpn. J. Appl. Phys. **28**, L2112 (1989).

[16] S. Nakamura, Jpn. J. Appl. Phys. **30**, L1705 (1991).

[17] S. Nakamura, T. Mukai, M. Senoh, and N. Iwasa, Jpn. J. Appl. Phys. **31**, L139 (1992).

[18] T. Nagatomo, T. Kuboyama, H. Minamino, and O. Omoto, Jpn. J. Appl. Phys. **28**, L1334 (1989).

[19] N. Yoshimoto, T. Matsuoka, T. Sasaki, and A. Katsui, Appl. Phys. Lett. **59**, 2251 (1991).

[20] S. Nakamura, and T. Mukai, Jpn. J. Appl. Phys. **31**, L1457 (1992).

[21] A. Koukitu, N. Takahashi, T. Taki, and H. Seki, Jpn. J. Appl. Phys. **35**, L673 (1996).

[22] A. Koukitu, N. Takahashi, T. Taki, and H. Seki, J. Cryst. Growth **170**, 306 (1997).

[23] S. Nakamura, N. Iwasa, and S. Nagahama, Jpn. J. Appl. Phys. **32**, L338 (1993).

[24] S. Nakamura, T. Mukai, M. Senoh, S. Nagahama, and N. Iwasa, J. Appl. Phys. **74**, 3911 (1993).

[25] S. Nakamura, T. Mukai, and M. Senoh, Appl. Phys. Lett. **64**, 1687 (1994).

[26] S. Nakamura, T. Mukai, and M. Senoh, J. Appl. Phys. **76**, 8189 (1994).

[27] S. Nakamura, M. Senoh, N. Iwasa, S. Nagahama, T. Yamada, and M. Mukai, Jpn. J. Appl. Phys. **34**, L797 (1995).

[28] S. Nakamura, M. Senoh, N. Iwasa, S. Nagahama, T. Yamada, and T. Mukai, Jpn. J. Appl. Phys. **34**, L1332 (1995).

[29] S. Nakamura, M. Senoh, S. Nagahama, N. Iwasa, T. Yamada, T. Matsushita, Y. Sugimoto, and H. Kiyoku, Appl. Phys. Lett. **69**, 4056 (1996).

[30] S. Nakamura, M. Senoh, S. Nagahama, N. Iwasa, T. Yamada, T. Matsushita, H. Kiyoku, Y. Sugimoto, T. Kozaki, H. Umemoto, M. Sano, and K. Chocho, Jpn. J. Appl. Phys. **37**, L309 (1998).

2. GaN Hetero-Epitaxial Growth by MOCVD Method

2.1 Introduction

GaN-based materials have a very good expectation for applications in high-performance devices such as high-density optical data storage, illumination and power electronics. However, the biggest barrier in the early years of GaN-based material growth is the non-existence of GaN substrate, which pushed researchers to rely on epitaxial growth on different substrate materials (hetero-epitaxy).

2.2 Comparison of Growth Substrate Materials for GaN-based Epitaxy

GaN growth has been widely performed on sapphire substrate due to its considerably good properties, which is stable at high temperature, having the same wurtzite crystal structure as GaN, and acceptable lattice and thermal mismatch with GaN. However, sapphire has a few limitations, such as its native physical property as an insulator which prevents fabrication of devices with vertical-type electrode structure. Sapphire also has a relatively low thermal conductivity which restricts thermal dissipation in high-power devices. Maximum diameter size for sapphire wafer is limited to 4 inches which limits mass-production quantity.

Hetero-epitaxy of GaN on 6H-SiC has been tremendously investigated by several groups [5,6], with successful fabrication of electronic and optoelectronic devices such as high electron mobility transistor (HEMT) [7], light emitting diode (LED) [8], and laser diode (LD) [9,10]. However, 6H-SiC substrate has limited availability,

restricted to small diameter size and relatively far more expensive than sapphire and Si substrate, which limits mass production quantity and interests for device fabrication.

Homo-epitaxy of GaN on free-standing GaN substrate has reached dislocation density as low as 10^6 cm^{-2} [11]. However, such substrate has maximum diameter size of only 2 inches and very limited availability, which pushes its price to become extremely expensive. Free-standing GaN substrate is only deployed in high-performance devices which need low dislocation density such as blue-violet LD.

While growth technology of GaN on sapphire, 6H-SiC and GaN free-standing substrate can be considered well established, there are demands for technological breakthrough for GaN-based epitaxy on Si substrate. Si substrate is widely available, having large diameter size of up to 12 inches, and very cost effective. The biggest advantage in successful growth of GaN-based materials on Si substrate is monolithic integration of GaN-based devices with well-established Si-based electronic devices such as integrated-circuits (ICs), photo-detectors (PDs), etc, allowing fabrication of multi-function hybrid device on a single wafer.

In contrast to sapphire, Si is a native semiconductor where electrical conductivity can be controlled by doping, allowing the fabrication of devices with vertical-type electrode structure. Si has better thermal conductivity than sapphire which improves thermal dissipation during high-temperature device operation (see Table II.I).

However, GaN epitaxy on Si substrate is more challenging than that of on sapphire or SiC substrates. Large thermal coefficient mismatch of 116% between GaN and Si is considered as the main reason for cracks to occur during cooling down after growth, even though lattice mismatch for GaN/Si(111) (-17%) is almost similar to GaN/sapphire (16%). Ga-Si reaction during growth causes amorphous meltback-etching

layer, and Si gas from the substrate causes low-doping density in p-type GaN epitaxial layer. These growth challenges have been addressed by many types of buffer layer techniques to obtain good quality GaN epitaxy on Si substrate.

GaN epitaxy on Si substrate has typical dislocation density of around 10^7 - 10^{11} cm^{-2} [12], and can still be improved by optimizing its growth techniques. However, as shown in Fig. 2.1, GaN grown on Si with low-temperature AlN buffer layer is more prone to cracks when the growth temperature is cooled down to room temperature (RT), due to large thermal expansion mismatch and lattice mismatch. In sapphire substrate, GaN epilayer undergo compressive strain when growth temperature is returned to RT. In contrast, GaN epilayer grown on Si substrate suffers tensile stress when growth temperature is cooled down to RT making Si substrate more prone to cracks compared to sapphire substrate for layer thicker than 1 μm.

This research concentrates on GaN epitaxy on Si substrate grown with high-temperature AlN nucleation layer and AlN/GaN multilayer (ML). Further improvement on material and optical properties have been achieved by insertion of $Al_{0.06}Ga_{0.94}N$/GaN cladding underlayer prior to growth of active layer for LED [13-14].

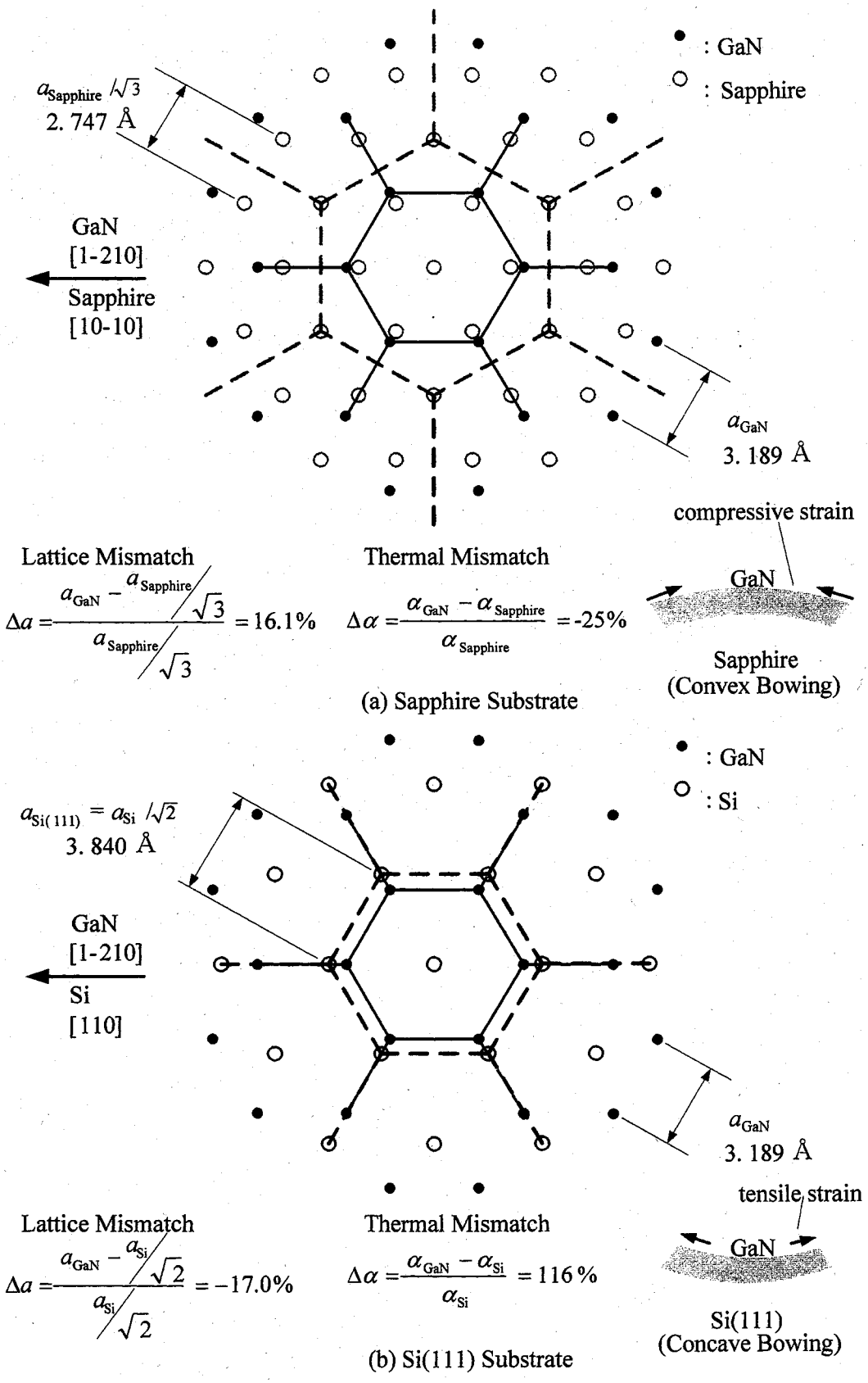

Fig. 2.1. Mechanism of lattice and thermal mismatch in GaN grown on (a) sapphire substrate and (b) GaN grown on Si(111) substrate.

Table II.I: Comparison of substrates for GaN epitaxial growth [1-4].

Substrate		Silicon (111)	Sapphire (0001)	6H-SiC	GaN (0001)
Cost		Very Low	High	Very High	Very High
Diameter Size		Very Large (6 inches)	Large (4 inches)	Small (2 inches)	Small (2 inches)
Lattice Constant (Å)	a	5.43	4.758	3.08	3.189
	c	-	12.991	15.12	5.185
Thermal Conductivity (W/cm K)		1.5	0.5	3.0-3.8	1.3
Thermal Expansion Coefficient (in-plane) ($\times 10^{-6}$/K)		2.59	7.5	4.2	5.59
Lattice Mismatch GaN/subst. (%)		-17	16	3.5	0
Thermal Mismatch GaN/subst. (%)		116	-25	33	0
Epitaxial Growth		Need Improvement	Good	Good	Best

2.3 GaN-based Epitaxy on Si Substrate

Buffer and intermediate layers have been extensively investigated by many research groups for GaN growth on Si substrate, such as AlN/AlGaN buffer and AlN/GaN multilayer (ML) [15-18], AlN interlayer [19] and Si_xN_{1-x} interlayer [20]. This research concentrates on crystal improvement for GaN epitaxy on Si substrate using AlN/AlGaN buffer and AlN/GaN ML intermediate layer. Different buffer and/or intermediate layer growth techniques, such as AlN interlayer [19], Si_xN_{1-x} interlayer [20], epitaxial lateral overgrowth (ELO) [21] and pendeo epitaxial overgrowth (PEO) [22] are not covered in this dissertation.

2.3.1 AlN/AlGaN Buffer Layer

AlN/AlGaN layer is used to prevent formation of meltback-etching when GaN is grown on Si substrate. AlN/AlGaN also acts as intermediate layer to create a high-density nucleation growth. For growth on sapphire substrate, high-density nucleation growth is achieved by low-temperature GaN buffer layer. However, for growth on Si substrate, low-temperature GaN buffer cannot be used due to Ga-Si reaction which results in amorphous meltback-etching layer. Therefore, materials such as AlN and AlGaN which are stable at high temperature are preferred for high-density nucleation growth. Usage of AlN layer as nucleation layer for GaN growth on Si substrate has been reported by many groups [23-28]. However, AlN layer growth suffers poor surface flatness, which influences the subsequent layer growth. There is report of 170 nm GaN layer grown on the initial AlN nucleation layer [29]. However, while it

depends on the Al composition, AlGaN has relatively better coating property and is easier to grow [30]. Therefore, AlGaN is considered as a good candidate for intermediate layer. Our research group has reported AlN/AlGaN buffer layer to take advantage of the combined material properties [15-18]. AlN layer which is stable at high-temperature is initially grown on Si substrate to create a high-density nucleation layer, followed by AlGaN layer to obtain a layer with good surface flatness.

2.3.2 AlN/GaN Multilayer (ML) Intermediate Layer

Multilayer (ML) and superlattice layer growth technology is very important to control crack generation in III-nitride-based semiconductor layer growth. In III-nitride layer growth on Si substrate, reactor temperature ramp-down to RT generates concave wafer curvature, and cracks on the epitaxial layer due to the difference of thermal expansion coefficient between Si substrate and III-nitride epitaxial layer, rendering growth for thick epitaxial layer to be difficult. Optimization in the epitaxial structure is necessary to successfully grow high-quality crack-free thick GaN-based layer on Si substrate. The necessity to grow thick epitaxial layer to improve the material quality has made ML intermediate layer an important factor in controlling wafer curvature and cracks. ML intermediate layer is also effective to reduce misfit dislocations resulted from lattice mismatch of GaN-based epitaxial layer and the underlying Si substrate. Threading dislocations (TDs) can be controlled to prevent them from penetrating to the surface using strained-layer superlattices (SLS), a method which has been used previously in GaAs-based growth on Si substrate [29,31,32]. When a stack of two types of material with different lattice constant is grown coherently, lattice strain is built upon

the interface of the two different materials giving a strong strain when they are accumulated together. Therefore, TDs which reach the interface are bent by the strain, and reaction between inclined TDs will create dislocation close-loop, eliminating the TDs from penetrating vertically into the epitaxial surface. The ML structure creates multiple built-up interface strain for TD inclination, thus, it is possible to control penetrations of TDs into the subsequent epitaxial layers. If the lattice strain is weak, it is not possible to bend the threading dislocations causing it to penetrate through the MLs. On the other hand, if the lattice strain is too large, new misfit dislocations might be built due to the strain. In this research, a ML consisting of periods of AlN and GaN stacks with respective layer thickness optimized at 5 nm and 20 nm is used as the fundamental intermediate layer, followed by further optimization in the succeeding layer.

2.4 Conclusions

This chapter describes buffer and intermediate layer growth techniques and their mechanism in improving crystal quality for GaN epitaxy on Si substrate. In our GaN growth method on Si substrate, a thin AlN nucleation layer is grown initially on the substrate to prevent meltback-etching due to Ga-Si reaction, followed by AlGaN layer to improve surface roughness. Subsequently, a stack of AlN/GaN ML is grown to suppress TDs, resulting in a high-quality GaN epitaxy in the succeeding layer. The techniques described here is the fundamental techniques for further improvement carried out through this research.

References

[1] S. Nakamura, S. Pearton, and G. Fasol, *The Blue Laser Diode*, Springer-Verlag, Berlin, Germany (2000).

[2] S. Nakamura, S. Chichibu, *Introduction to Nitride Semiconductor Blue Lasers and Light Emitting Diodes*, Taylor & Francis, New York, USA (2000).

[3] J. Piprek, *Nitride Semiconductor Devices Principles and Simulation*, Wiley-VCH Verlag, Weinheim, Germany (2007).

[4] K. Takahashi, *Wide-Gap Semiconductor Optical and Electronic Devices* (in Japanese: ワイドギャップ半導体光・電子デバイス), Morikita Publishing, Tokyo, Japan (2006).

[5] M. A. L. Johnson, S. Fujita, W. H. Rowland, K. A. Bowers, W. C. Hughes, Y. W. He, N. A. El-Masry, J. W. Cook, J. F. Schetzina, J. Ren, and J. A. Edmond, J. Vac. Sci. Technol. B **14**, 2349 (1996).

[6] J. T. Torvik, M. Leksono, J. I. Pankove, B. V. Zeghbroeck, H. M. Ng, and T. D. Moustakas, Appl. Phys. Lett. **72**, 1371 (1998).

[7] J. Bernát, M. Wolter, A. Fox, M. Marso, J. Flynn, G. Brandes, and P. Kordoš, Electron Lett. **40**, 78 (2004).

[8] H. S. Kong, M. Leonard, G. Bulman, G. Negley, and J. Edmond, Mat. Res. Soc. Symp. Proc. **395**, 903 (2005).

[9] A. Kuramata, K. Hirino, and K. Domen, Fujitsu Sci. Tech. J. **34**, 191 (1998).

[10] J. Edmond, A. Abare, M. Bergman, J. Bharathan, K. L. Bunker, D. Emerson, K. Haberern, J. Ibbetson, M. Leung, P. Russel, and D. Slater, J. Cryst. Growth **272**, 242 (2004).

[11] S. Hashimoto, Y. Yoshizumi, T. Tanabe, and M. Kiyama, J. Cryst. Growth **298**, 871 (2006).

[12] Y. B. Pan, Z. J. Yang, Z. T. Chen, Y. Lu, T. J. Yu, X. D. Hu, K. Xu, and G. Y. Zhang, J. Cryst. Growth **286**, 255 (2006).

[13] B. A. B. A. Shuhaimi, T. Suzue, Y. Nomura, Y. Maki, and T. Egawa, Mater. Res. Soc. Symp. Proc. **1167**, O02-05 (2009).

[14] B. A. B. A. Shuhaimi, P. C. Khai, T. Suzue, Y. Nomura, and T. Egawa, Mater. Res. Soc. Symp. Proc. **1167**, O04-01 (2009).

[15] T. Egawa, B. Zhang, N. Nishikawa, H. Ishikawa, T. Jimbo, and M. Umeno, J. Appl. Phys. **91**, 528 (2002).

[16] H. Ishikawa, K. Asano, B. Zhang, T. Egawa, and T. Jimbo, Phys. Stat. Sol. A **201**, 2653 (2004).

[17] T. Egawa, B. Zhang, and H. Ishikawa, IEEE Elect. Dev. Lett. **26**, 169 (2005).

[18] B. Zhang, T. Egawa, H. Ishikawa, Y. Liu, and T. Jimbo, Jpn. J. Appl. Phys. **42**, L226 (2003).

[19] A. Dadgar, Jpn. J. Appl. Phys. **39**, L1183 (2000).

[20] T. Riemann, T. Hempel, J. Christen, P. Veit, R. Clos, A. Dadgar, A. Krost, U. Haboeck, and A. Hoffman, J. Appl. Phys. **99**, 123518 (2006).

[21] E. Feltin, B. Beumont, P. Vennéguès, M. Vaille, P. Gibart, T. Riemann, J. Christen, L. Dobos, and B. Pécz, J. Appl. Phys. **93**, 182 (2003).

[22] T. Gehrke, K. J. Linthicum, E. Preble, P. Rajagopal, C. Ronning, C. Zorman, M. Mehregany, and R. F. Davis, J. Electron. Mater. **29**, 306 (2000).

[23] A. Watanabe, T. Takeuchi, and K. Hirosawa, J. Cryst. Growth **128**, 391 (1993).

[24] A. Ohtani, K. S. Stevens, and R. Beresford, Appl. Phys. Lett. **65**, 61 (1994).

[25]P. Kung, A. Saxler, X. Zhang, D. Walker, T. C. Wang, I. Ferguson, and M. Razeghi, Appl. Phys. Lett. **66**, 2958 (1995).

[26]M. Godlewski, J. P. Bergmann, B. Monemar, U. Rossner, and A. Barski, Appl. Phys. Lett. **69**, 2089 (1996).

[27]J. M. Redwing, J. S. Flynn, M. A. Tischler, W. Mitzchel, and A. Saxler, Mater. Res. Soc. Symp. Proc. **395**, 201 (1996).

[28]F. Widmann, B. Daudin, G. Feuillet, Y. Samson, M. Arlery, and J. L. Rouviere, MRS Internet J. Nitride Semicond. Res. **2**, 20 (1997).

[29]H. P. D. Schenk, E. Feltin, M. Laugt, O. Tottereau, P. Vennegues, and E. Dogheche, Appl. Phys. Lett. **83**, 5139 (2003).

[30]K. Hirosawa, K. Hiramatsu, N. Sawaki, and I. Akasaki, Jpn. J. Appl. Phys. **32**, L1039 (1993).

[31]T. Soga, S. Hattori, S. Sakai, M. Takeyasu, and M. Umeno, J. Appl. Phys. **57**, 4578 (1985).

[32]A. Georgakilas, and A. Christou, J. Appl. Phys. **76**, 7332 (1994).

3. Characterization Methods for GaN-based Epitaxy and Light Emission Devices

3.1 Introduction

Thin film characterization method is important to understand the mechanisms in GaN-based crystal such as lattice defects, and photonic transitions in the band-gap. A proper understanding in the crystal level allows easier control of parasitic properties, hence, allows for optimization in growth parameters to improve GaN epitaxial quality.

3.2 Characterization of Lattice Defects[26]

Most of GaN-based optoelectronics and electronic devices are hetero-epitaxially grown on third party substrate such as sapphire, SiC, and Si. However, lattice mismatch and thermal expansion coefficient mismatch with the substrate produces large quantity of lattice defects in the GaN crystal. The lattice defect modifies active layer growth pattern, alters optical properties, and deteriorates device operating characteristics and its lifetime reliability. Thus, understanding the characteristics of lattice defect is essential to control or remove the defects.

In a conventional high-quality GaN film grown on c-face sapphire or SiC substrate using AlN or GaN buffer layer by metal organic chemical vapor deposition (MOCVD) [1,2], the first 100 nm thickness after the hetero-epitaxial interface between GaN and sapphire shows large quantity of stacking faults and c-face defects to relax the

layer. However, after the initial 100 nm thickness, all other types of lattice imperfections disappear, leaving only threading dislocations (TDs) with density around $10^8 - 10^{10}$ cm^{-2} [3-5].

Lattice defects can be classified into point-defect, line-defect (dislocation), and face-defect. In GaN film, the particular type of lattice defect observed is line defect (dislocation), which largely influences device characteristics.

Line defect can be classified into edge-dislocation, screw-dislocation, and mixed-dislocation [6]. Figure 3.1 shows the mechanism of edge-dislocation and screw-dislocation in c-plane GaN. In edge-dislocation, dislocation line and Burgers vector are in perpendicular direction, while in screw-dislocation, the dislocation line and Burgers vector are in parallel direction. Edge-dislocation occurs due to excess lattice penetration on $(11\bar{2}0)$ face, with Burgers vector in $\boldsymbol{b} = 1/3 < 11\bar{2}0 >$ direction. On the other hand, screw-dislocation occurs due to partial atomic step, with Burgers vector $\boldsymbol{b} =< 0001 >$. Mixed-dislocation is a mix of edge-dislocation and screw-dislocation, with Burgers vector $\boldsymbol{b} = 1/3 < 11\bar{2}3 >$. The line-defect described in this section is for hexagonal crystal structure, which occurs when epitaxial growth is performed on c-face. GaN crystal structure exists in cubic zincblende structure and hexagonal wurtzite structure. However, the wurtzite structure is the meta-stable structure for GaN.

3.2.1 X-Ray Diffraction (XRD) Method

X-ray diffraction (XRD) ω-scan method is conventionally used to characterize structural quality of a GaN crystal, because density of line defect influence the ω-scan

full-width at half-maximum (FWHM) line width. Increase of screw component and mixed component of the dislocation density increases tilt component in c-plane GaN, and therefore increases FWHM line width of symmetric reflection in (0002) and (0004) diffraction peak. Meanwhile, increase of edge component and mixed component of the dislocation density increases twist component of c-plane GaN, and therefore increases FWHM line width of asymmetric reflection.

3.2.2 Transmission Electron Microscopy (TEM) Method

Characteristics of line defects can be analyzed by transmission electron microscopy (TEM). However, a proper method and time is necessary for sample preparation, prior to actual cross-sectional TEM observation. In cross-sectional TEM observation, when inversed lattice vector is $\boldsymbol{g}$, and Burgers vector for line defects is $\boldsymbol{b}$, line defects can be classified using $\boldsymbol{g} \times \boldsymbol{b} = 0$ invisibility criterion. Specifically, when $\boldsymbol{g} = <11\bar{2}0>$, Burgers vector $\boldsymbol{b} = <0001>$ that is perpendicular to this direction will eliminate visibility of screw dislocation component, showing only edge dislocation and mixed dislocation components. In $\boldsymbol{g} = <0002>$ direction, Burgers vector $\boldsymbol{b} = 1/3 <11\bar{2}0>$ at perpendicular direction will eliminate visibility of edge dislocation component, showing only screw dislocation and mixed dislocation components. Screw dislocation density is normally lower relative to that of edge dislocation density.

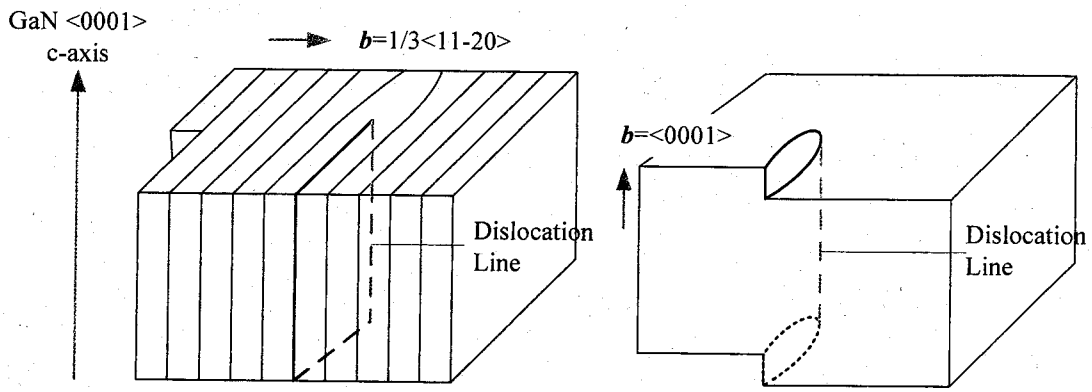

(a) Edge Dislocation (b) Screw Dislocation

Fig. 3.1. Mechanism of edge dislocation and screw dislocation.

3.3 Luminescence Properties[27]

The elementary excitation process of semiconductors over its band-gap energy first creates free electrons in the conduction band, and holes in the valence band. Subsequently, they lose energy and momentum, i.e. relax, to the lowest energy states by emitting phonons in general. They then form a quasi-particle that is a bound state with Coulomb interaction in between the electron and the hole. The quantum of this electronic polarization is called exciton.

In semiconductors, a weakly bound electron-hole (e-h) pair whose wave-function propagates more than the lattice spacing is formed and is called as Mott-Wannier exciton. Conversely, in ionic crystals or molecular crystals, e-h pair is strongly bound at the matrix atom or localized at its neighborhood, which is called as Frenkel exciton. Wannier excitons can freely move in the crystal in a form of mobile, bound e-h pair, which is called as free exciton (FE) [7]. Thus, they do not contribute to the electrical conductivity. However, they play an important role in optical absorption, reflection, and emission processes in semiconductors. The energy states of excitons resemble those of shallow impurities. The electron turns around the hole like hydrogen atom, but in the material with dielectric constant $\varepsilon = \varepsilon_S \varepsilon_0$.

Studies on the exciton resonance structures in GaN began at the beginning of 1970s. Due to the crystal symmetry and relatively weak spin-orbit interaction, the valence band of the wurtzite hexagonal GaN (h-GaN) is lifted to three separate bands [8-9], as shown in Fig. 3.2. Dingle at al. [10] have assigned the energies of three (A, B and C) excitons related to transitions from the separate valence band (Γ_{9v}, Γ_{7v}, and Γ_{7v} in Fig. 3.2.) to the conduction band (Γ_{7c}) band, as $E_{ex}(\mathrm{A}) = 3.474 \pm 0.002$ eV,

$E_{ex}(B) = 3.480 \pm 0.002$ eV, and $E_{ex}(C) = 3.501 \pm 0.01$ eV by means of the polarized optical reflectance (OR) measurements at 2 K after Pankove *et al.* [11] observed a strong photoluminescence (PL) peak at 3.477 eV at 1.6 K. Monemar [12] has also reported the exciton energy from photoluminescence excitation (PLE) spectra at 1.6 K as $E_{ex}(A) = 3.4751 \pm 0.0005$ eV, $E_{ex}(B) = 3.481 \pm 0.001$ eV, and $E_{ex}(C) = 3.493 \pm 0.005$ eV, and he deduced exciton binding energy, E_b of the ground state A-exciton as 28 meV from the E_g and $E_{ex}(A)$ values. Amano *et al.* [13] and Logothetidis *et al.* [14] have suggested a contribution of excitons in the optical absorption (OA) spectra of zinc-blende cubic GaN (c-GaN) and h-GaN up to room-temperature (RT). Shan *et al.* [15-16] have also assigned modulation photo-reflectance (PR) signals to exciton resonance structures up to RT.

Typical radiative recombination processes occurring in semiconductors are schematically summarized in Fig. 3.3. In general, luminescence spectra of high purity, high quality semiconductors are dominated by free exciton (FE) emission at low temperature. The FE emission from wurtzite GaN at low temperature has been observed in the early 1970s by Pankove *et al.* [11] and Dingle *et al.* [10]. There are various forms of exciton complex that are composed of exciton(s) and other particles [17]. Neutral donor has an outer electron, which turns around the donor ion with larger orbit diameter. It binds a free hole at the position where the static dipole between the hole and the neutral donor balances and then charge neutrality of the complex is satisfied. This complex is an exciton bound to a neutral donor (I_2) and is in general called a bound exciton (BE). Neutral acceptor also produces the bound exciton (I_1). Similarly, ionized donor and acceptor can produce excitons bound to them. The transition energy of BEs associated with neutral impurities is lower than that of FEs by their localization energy,

E_{loc}, which is nearly one tenth of the impurity ionization energy, E_a [18]. The relation between E_a and E_{loc} changes depend on material [19]. As E_{loc} is very small, BE recombination is dominant at very low temperatures and FE emission dominates the emission spectrum at intermediate temperatures between 20 K and 100 K in general depending on the stability of excitons in the matrix. Another process involving excitons at low temperature is a formation of exciton-polariton, which is a complex between the electromagnetic (photons) and excitons (or oscillators) that have the same resonance frequency as the photons at finite value of very small wave vector, k [20-22]. The contribution of exciton-polariton in optical spectra of wurtzite GaN was reported by Gil et al. [17,18] and Stepniewski et al. [19]. Excitons couple with several kind of phonons. A remarkable feature of the PL spectrum of GaN at low temperature is the appearance of longitudinal optical (LO) phonon replicas of FE and BE lines [10]. In impurity doped semiconductors, emission due to recombination of free carriers (electrons or holes) and the impurity levels (acceptors or donors) are dominant at intermediate temperature or RT depending on E_a of the impurity. They are referred to as free-to-bound (FB) or bound-to-free (BF) emissions. The simultaneous existence of donor and acceptor impurities introduce a pair type emission between them, and is called donor-acceptor pair (DAP) recombination. The band-to-band (BB) emission occurs in direct band-gap semiconductors with relatively high temperature, high carrier density, small exciton binding energy, E_b, or high number of active phonons which produce free carriers.

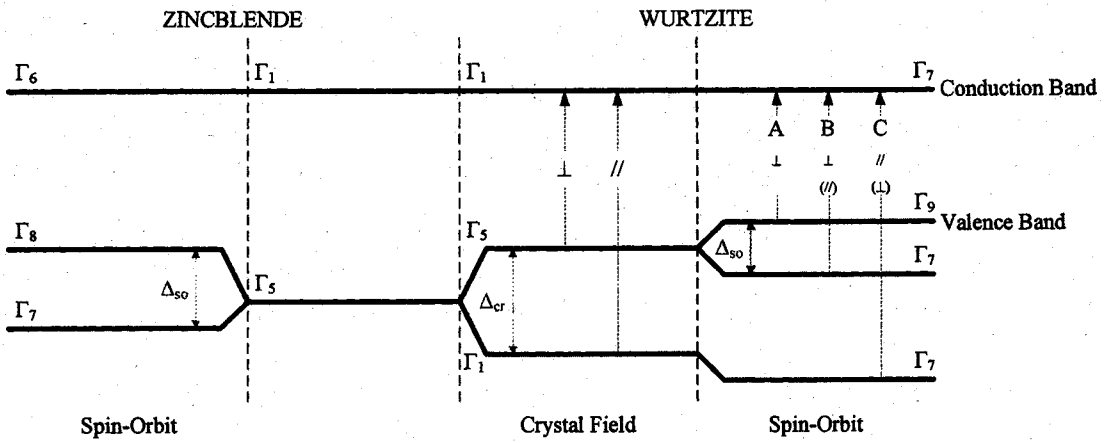

Fig. 3.2. Band structures and labeling of respective transition in zincblende and wurtzite GaN. The indications ⊥ and // show that the transition is allowed for the light polarization *E* perpendicular and parallel to the optic (c) axis. Parentheses means that the transition is partially allowed. The value Δ_{so} and Δ_{cr} are the spin-orbit and crystal field splitting, respectively.

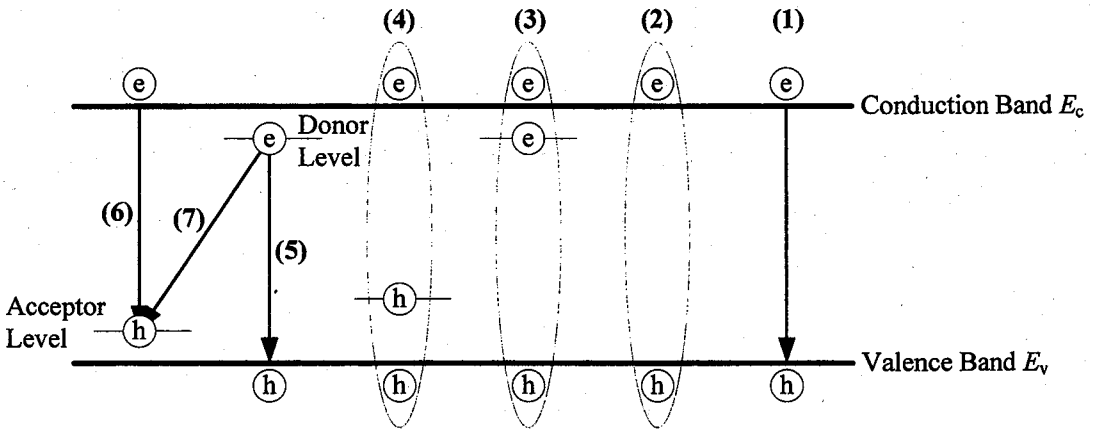

(1) Band-to-band (BB) emission
(2) Free exciton (FE) emission
(3) Neutral donor bound exciton (BE) emission (I_2)
(4) Neutral acceptor bound exciton (BE) emission (I_1)
(5) Bound-to-free (BF) emission
(6) Free-to-bound (FB) emission
(7) Donor-acceptor pair (DAP) emission

Fig. 3.3. Schematic drawing of radiative and recombination processes in semiconductors preferably at low temperature where the excitonic and impurity-related emission occur.

3.4 Internal, Extraction, External, and Power Efficiencies[28]

In a semiconductor crystal, several mechanisms for non-radiative recombination exist, including Shockley-Read, Auger, and surface recombination. Even though non-radiative recombination can be reduced, it can never be totally eliminated. Any semiconductor crystal has some native defects. Even though the concentration of these native defects can be low, it is never zero. Thermodynamic considerations predict that if an energy E_a is needed to create a specific point defect in a crystal lattice, the probability that such a defect does indeed form at a specific lattice site, is given by the Boltzmann factor, i.e. $\exp(-E_a/kT)$. The product of the concentration of lattice sites and the Boltzmann factor gives the concentration of defects. A native point defect or extended defect may form a deep state in the gap and thus be a non-radiative recombination center.

If radiative lifetime in a semiconductor crystal is denoted as τ_r and non-radiative lifetime is denoted as τ_{nr}, the total probability of recombination is given by the sum of the radiative and non-radiative probabilities,

$$\tau^{-1} = \tau_r^{-1} + \tau_{nr}^{-1} \tag{3.1}$$

The relative probability of radiative recombination is given by the radiative probability over the total probability of recombination. Thus, the probability of radiative recombination or **internal quantum efficiency** (η_{iqe}) is given by,

$$\eta_{iqe} = \frac{\tau_r^{-1}}{\tau_r^{-1} + \tau_{nr}^{-1}} \tag{3.2}$$

The η_{iqe} gives the ratio of the number of light quanta emitted inside the semiconductor to the number of charge quanta undergoing recombination.

In device evaluation viewpoint, active region of an ideal LED emits *one photon* for *every electron* injected. Each charge quantum-particle (electron) produces one light quantum-particle (photon). Thus, the ideal active region of an LED has a *quantum efficiency* of unity. The η_{iqe} is defined as,

$$\eta_{iqe} = \frac{\text{Number of photons emitted from active region per second}}{\text{Number of electrons injected into LED per second}} = \frac{P_{int}/(h\upsilon)}{I/e} \tag{3.3}$$

where P_{int} is the optical power emitted from the active region and I is the injection current.

In an ideal LED, all photons emitted by the active region are also emitted into free space. Such an LED has unity *extraction efficiency*. However, in real LED, only partial of the optical power is emitted into free space. Some photons may never leave the semiconductor die, due to several possible loss mechanisms. For example, light emitted by the active region can be reabsorbed in the substrate of the LED, assuming that the substrate is absorbing at the emission wavelength. This problem is crucial for wide band-gap InGaN-based LED grown in narrower band-gap Si substrate. Emitted light may be incident on a metallic contact surface and be absorbed by the metal. In addition, the phenomenon of *total internal reflection*, also referred as *trapped light phenomenon*, reduces the ability of the light to escape from the semiconductor. Light ***extraction efficiency*** (η_{ext}) is defined as,

$$\eta_{ext} = \frac{\text{Number of photons emitted into free space per second}}{\text{Number of photons emitted from active region per second}} = \frac{P/(h\upsilon)}{P_{int}/(h\upsilon)} \tag{3.4}$$

where P is the optical power emitted into free space.

The η_{ext} can be a severe limitation for high-performance LEDs. It is quite

difficult to increase the η_{ext} beyond 50% without resorting to highly sophisticated and costly device processes.

The ***external quantum efficiency*** (η_{eqe}) is defined as,

$$\eta_{eqe} = \frac{\text{Number of photons emitted into free space per second}}{\text{Number of electrons injected into LED per second}} = \frac{P/(h\upsilon)}{I/e} = \eta_{iqe}\eta_{ext} \tag{3.5}$$

The η_{ext} gives the ratio of the number of useful light particles to the number of injected charge particles.

The ***power efficiency*** (η_{power}) is defined as,

$$\eta_{power} = \frac{P}{IV} \tag{3.6}$$

where IV is the electrical power provided to the LED. The power efficiency (η_{power}) is also called *wall plug efficiency*.

3.5 Conclusions

This chapter describes the fundamental characterization method for GaN-based epitaxy. Lattice defects mechanism in GaN film is briefly explained, including the characterization methods using XRD and TEM which is the common method to evaluate GaN crystal quality. Luminescence properties from GaN film is also described, which is important to evaluate GaN crystal quality. The internal, external, extraction and power efficiencies are important factor to evaluate light emission devices such as LED.

References

[1] H. Amano, N. Sawaki and I. Akasaki, Appl. Phys. Lett. **48**, 353 (1986).

[2] S. Nakamura, Jpn. J. Appl. Phys. **30**, L1705 (1991).

[3] S. D. Lester, F. A. Ponce, M. G. Craford and D. A. Steigerwald, Appl. Phys. Lett. **66**, 1249 (1995).

[4] W. Qian, M. Skowronski, M. D. Graef, K. Doverspike, L. B. Rowland and D. K. Gaskill, Appl. Phys. Lett. **66**, 1252 (1995).

[5] X. H. Wu, L. M. Brown, D. Kapolnek, S. Keller, B. Keller, S. P. DenBaars and J. S. Speck, J. Appl. Phys. **80**, 3228 (1996).

[6] T. Hino, S. Tomiya, T. Miyajima, K. Yanashima, S. Hashimoto and M. Ikeda, Appl. Phys. Lett. **76**, 3421 (2000).

[7] G. H. Wannier, Phys. Rev. **52**, 191 (1937).

[8] G. Dresselhaus, Phys. Rev. **105**, 135 (1957).

[9] J. J. Hopfield, J. Phys. Chem. Solids **15**, 97 (1960).

[10] R. Dingle, D. D. Sell, S. E. Stokowski and M. Ilegems, Phys. Rev. B **4**, 1211 (1971).

[11] J. I. Pankove, J. E. Berkeyheiser, H. P. Maruska and J. Wittke, Solid State Commun. **8**, 1051 (1970).

[12] B. Monemar, Phys. Rev. B **10**, 676 (1974).

[13] H. Amano, N. Watanabe, N. Koide and I. Akasaki, Jpn. J. Appl. Phys. **32**, L1000 (1993).

[14] S. Logothetidis, J. Petalas, M. Cordona and T. D. Moustakas, Mat. Sci. Eng. B **29**, 65 (1995).

[15] W. Shan, T. J. Shmidt, X. H. Yang, S. J. Hwang, J. J. Song and B. Goldenberg, Appl. Phys. Lett. **66**, 985 (1995).

[16] W. Shan, T. J. Shmidt, X. H. Yang, J. J. Song and B. Goldenberg, J. Appl. Phys. **79**, 3691 (1996).

[17] M. A. lampert, Phys. Rev. Lett. **1**, 450 (1958).

[18] J. R. Haynes, Phys. Rev. Lett. **4**, 361 (1960).

[19] H. B. Bebb and E. Williams, *Semiconductor and Semimetals*, eds. R. K. Willardson and A. C. Beer, Academic, New York, USA, **8**, 182-392 (1972).

[20] Y. Toyozawa, Prog. Theor. Phys. Suppl. **12**, 111 (1959).

[21] J. J. Hopfield, *II-VI Semiconducting Compunds*, W. A. Benjamin, New York, USA, p. 786 (1967).

[22] W. C. Tait, D. A. Cambell, J. R. Packard and R. L. Weiher, *II-VI Semiconducting Compounds*, W. A. Benjamin, New York, USA, p. 370 (1967).

[23] B. Gil, S. Clur and O. Briot, Solid State Commun. **104**, 267 (1997).

[24] B. Gil and O. Briot, Phys. Rev. B **55**, 2530 (1997)

[25] K. Stepniewski, K. P. Korona, A. Wysmolek, J. M. Baronowski, K. Pakula, G. Martinez, I. Gregory and S. Porowski, Phys. Rev. B **56**, 15151 (1997).

[26] K. Takahashi, Wide-Gap Semiconductor Optical and Electronic Devices (in Japanese: ワイドギャップ半導体光・電子デバイス), Morikita Publishing, Tokyo, Japan (2006).

[27] S. Nakamura and S. F. Chichibu, *Introduction to Nitride Semiconductor Blue Lasers and Light Emitting Diodes*, Taylor & Francis, New York, USA, p. 154-165 (2000).

[28] E. F. Schubert, *Light-Emitting Diodes*, Cambridge University Press, New York,

USA, p. 44 (2003).

[29] J. Piprek, *Nitride Semiconductor Devices Principles and Simulation*, Wiley-VCH, Weinheim, Germany (2007).